Two-Dimensional Infrared Correlation Spectroscopy as a Probe of Sequential Events in the Thermal Unfolding of Cytochromes *c*[†]

Angelo Filosa,[‡] Yan Wang,[§] Ashraf A. Ismail,*[,§] and Ann M. English*[,‡]

Department of Chemistry and Biochemistry, Concordia University, 1455 de Maisonneuve Boulevard West, Montreal, Quebec, Canada H3G 1M8, and McGill IR Group, Department of Food Science and Agricultural Chemistry, McGill University, 21111 Lakeshore Road, Ste. Anne de Bellevue, Quebec, Canada H9X 3V9

Received November 28, 2000; Revised Manuscript Received April 12, 2001

ABSTRACT: The sequential unfolding events of horse, cow, and tuna ferricytochromes *c* (cyt *c*) as a function of increasing temperature over the range 25−81 °C were investigated by resolution-enhanced two-dimensional infrared (2D IR) correlation spectroscopy. The 2D IR analysis revealed that in the thermal denaturation of the two mammalian cyts, the overall sequence of unfolding is similar, with denaturation of extended-chain and turn structures occurring prior to unfolding of α-helices, followed by denaturation of residual stable extended-chain structures. In tuna cyt *c*, denaturation of all extended-chain structures precedes the unfolding of α-helices. Moreover, in cow cyt *c*, unfolding of all helical components occurs as one cooperative unit, but in horse and tuna cyts *c*, the helical components behave as subdomains that unfold separately, as proposed recently by Englander and co-workers for horse cyt *c* [Bai et al. (1995) *Science 269*, 192−197; Milne et al. (1999) *J. Mol. Biol. 290*, 811−822]. At higher temperatures, following the loss of secondary structure, protein aggregation occurs in the three cyts *c*. The data presented here establish that variations in the thermal unfolding of cyts *c* can be associated with specific sites in the protein that influence local flexibility yet have little affect on global stability. This study demonstrates the power of resolution-enhanced 2D IR correlation spectroscopy in probing unfolding events in homologous proteins.

Ferricytochrome *c* (cyt *c*)[1] mediates the transfer of electrons from cyt *c* reductase to cyt *c* oxidase in the electron transport chain of eukaryotes (*1*−*3*). X-ray analysis of horse cyt *c* (Figure 1) reveals a single polypeptide chain organized into five α-helical segments (yellow) interconnected by six *β*-turns (green) and extended-chain structures (blue), which account for ∼45, 25, and 30% of its amino acid residues, respectively. X-ray and nuclear magnetic resonance (NMR) data for horse and tuna cyts *c* reveal that both proteins possess remarkably similar main-chain structures (*2*, *4*−*6*). Cow cyt *c* is assumed to be essentially identical in structure to horse cyt *c* since the two proteins share high sequence identity (>97%). Notwithstanding the overall similar structural elements, the proteins exhibit significant differences in local stabilities as probed by tryptic digestion (*7*−*9*), Fourier transform infrared (FTIR) spectroscopy (*10*), and

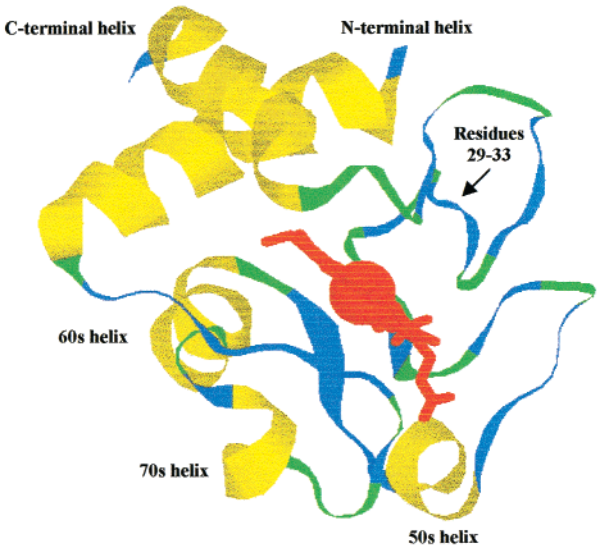

FIGURE 1: Horse heart cyt *c* C_α backbone with its heme (red), helical (yellow), turns (green), and extended-chain (blue) structures. The model was generated using Rasmol and the crystal structure coordinates from Protein Data Bank entry 1HRC (*2*).

695-nm absorption (*7*, *11*−*13*). However, global conformational stabilities, as monitored by circular dichroism (*8*), calorimetry (*14*), and FTIR (*10*), are remarkably similar for cyts *c*.

To probe the different local stabilities observed for cyts *c*, FTIR spectroscopy was used to obtain information at the level of secondary structure from curve-fitting of the amide

[†] This research was supported by grants from the Natural Sciences and Engineering Research Council (NSERC) of Canada to A.M.E. and A.A.I., and by scholarships from the Fonds pour la Formation des Chercheurs et L'Aide à la Recherche (FCAR) of Quebec and the J. W. McConnell Memorial Graduate Fellowship (Concordia University) to A.F.

* Corresponding authors. A.M.E.: Phone (514) 848-3338, Fax (514) 848-2868, E-mail english@vax2.concordia.ca. A.A.I.: Phone (514) 398-7991, Fax (514) 398-7977, E-mail ashraf.ismail@mcgill.ca.

[‡] Concordia University.

[§] McGill University.

[1] Abbreviations: 2D IR, two-dimensional infrared; cyt *c*, ferricytochrome *c*; FSD, Fourier self-deconvolution; FTIR, Fourier transform infrared; H/D, hydrogen/deuterium; HWHH, half-width-at-half-height; NMR, nuclear magnetic resonance; T_m, transition-midpoint temperature.

10.1021/bi002710n CCC: $20.00 © 2001 American Chemical Society
Published on Web 06/19/2001

I (H_2O) and amide I′ (D_2O) bands (*10*). Essentially identical secondary structural elements were observed in horse and cow cyt *c*, whereas splitting of the α-helical absorption in tuna cyt *c* indicated the presence of less stable helical structures. Monitoring the FTIR amide I′ bands of the cyts *c* as a function of temperature revealed that loss of secondary structure and protein aggregation occurred within a narrow range (<10 °C). To determine whether sequential events are involved in thermal unfolding of the cyts *c*, we have reexamined our FTIR data (*10*) using generalized 2D IR correlation analysis (*15*), which is capable of detecting minor structural changes in response to external perturbations such as temperature (*16*, *17*). For example, 2D IR analysis revealed that the Cro repressor protein forms stable intermediates only after specific secondary structures are unfolded first, which was not observed from simple Fourier self-deconvolution (FSD) analysis (*16*). Likewise, Wang and coworkers (*18*) observed ovalbumin protein peaks by 2D IR that were detected in neither the raw nor the second-derivative spectra. The present 2D IR analysis of the thermal denaturation of cyts *c* reveals that the sequence of events in the unfolding of structurally homologous proteins can vary significantly.

EXPERIMENTAL PROCEDURES

IR Spectroscopy. FTIR spectra were recorded previously for cyts *c* from horse (Type VI) and cow and tuna (Type XI) (Sigma) (*10*). Typically, after hydrogen/deuterium (H/D) exchange was complete, 8 μL of a 4 mM cyt *c* solution in 50 mM sodium phosphate buffer (pD 7.0) containing 0.2 M KCl was sandwiched between two CaF_2 windows (Wilmad) separated by a 56-μm Teflon spacer (Harrick Scientific). Spectra were recorded on a Nicolet Magna IR 550 Series II FTIR spectrometer equipped with a deuterated triglycine sulfate KBr detector. The cell temperature was increased by 2 °C between 25 and 95 °C, and the FTIR spectrum was collected after the cell was thermally equilibrated for 10 min. Spectra represent an average of 256 scans recorded at a resolution of 2 cm^{-1} using a Happ−Genzel apodization with a velocity and aperture of 0.9494 cm/s and 67, respectively. To improve band resolution, FSD of the amide I′ bands was carried out using Omnic 3.1 software (Nicolet), employing a half-width-at-half-height (HWHH) of 13 cm^{-1} with an enhancement (*K* factor) of 2.

2D IR Analysis. Generalized 2D IR correlation analysis of the FSD amide I′ (1600−1700 cm^{-1}) spectra taken every 4 °C between 25 and 81 °C was carried out as described previously (*10*) using KG2D software written by Wang (*18*). A 5% correlation-intensity cutoff was used to generate both low- and high-resolution 2D IR plots for all three cyts *c*, and 2D analysis performed on duplicate sets of FTIR thermal denaturation spectra resulted in reproducible 2D correlation plots. The KG2D software can process any spectral data (e.g., Raman scattering, infrared, or ultraviolet/visible absorption) that can be imported by Grams/32 4.01 software (Galactic). Moreover, the change in the spectroscopic signal can be due to any physical variable, such as temperature (used here), time, pressure, or denaturant concentration. The advantage of using the KG2D software is that it allows 3D representations of the 2D contour maps to be examined using Grams/3D 3.02 software (Galactic). Rotating and zooming the 3D image aids in the identification of weak peaks in the 2D maps. However, caution must be exercised when generating 2D synchronous and asynchronous contour maps from spectra subjected to resolution-enhancement algorithms such as FSD. In particular, overdeconvolution can give rise to artifacts in the deconvolved spectra that can be easily misinterpreted as amide I′ band components (*19*). In the present work, a signal-to-noise ratio in the amide I′ absorption region of >25 000:1 and a residual water vapor absorption of <0.1 milliabsorbance unit were established as criteria for FSD. As suggested by Jackson and Mantsch (*20*), the absence of artifacts in the deconvolved spectra was verified by confirming that the number of bands and their positions in the deconvolved spectra matched those in second-derivative spectra generated from the same raw spectral data.

Interpretation of 2D IR Correlation Plots. Two types of 2D correlation plots are generated, synchronous and asynchronous, which represent the in-phase and out-of-phase variation, respectively, between spectral components to an applied perturbation. The asynchronous contour plot combined with the synchronous plot provides details on the sequence of events following an applied perturbation. As a result of the symmetric and antisymmetric properties of the cross-correlation peaks with respect to the diagonal line in the 2D plots, only peaks above the diagonal are discussed. Peaks are identified as *X* vs *Y* cm^{-1}, where *X* and *Y* represent the frequencies marked on the *x*- and *y*-axes, respectively. Throughout this paper, solid and dashed lines in the 2D plots denote positive and negative correlation peaks, respectively. According to the rules proposed by Noda (*15*), the sign of a cross-peak (positive or negative) in the asynchronous plots determines the sequential relationship between two bands. When the system is perturbed by increasing the temperature, as in the present study, a positive region in the asynchronous map indicates that the spectral intensity change at *X* occurs at a lower temperature than that at *Y* if the corresponding synchronous peak at *X* vs *Y* is also positive. On the other hand, if the synchronous peak at *X* vs *Y* is negative, the spectral intensity change at *X* occurs at higher temperature than that at *Y*. A negative peak in the asynchronous map is interpreted in a similar manner; i.e., *X* changes at higher (lower) temperature if the synchronous *X* vs *Y* peak is positive (negative).

RESULTS AND DISCUSSION

Thermal Unfolding of Horse, Cow, and Tuna Cyts c. Prior to reporting the 2D IR analysis of the thermal denaturation of cyts *c*, the previous 1D analysis will be summarized (*10*). Curve-fitting of the FSD amide I′ spectra of horse and cow cyts *c*, which consisted of four bands (1671, 1653, 1641, and 1631 cm^{-1}), revealed similar secondary structural elements. Bands attributed to α-helices, at 1653 cm^{-1} in horse and cow cyts *c*, and at 1654 and 1645 cm^{-1} in tuna cyt *c*, decrease in intensity with increasing temperature (Figure 2a−c). Splitting of the α-helical absorption into two populations (1654 and 1645 cm^{-1}) in tuna cyt *c* reveals the presence of less stable helical structures (*10*), that likely include the 60s helix (residues 61−70) based on NMR data (*4*, *6*). Loss of absorption in horse and cow by turns at 1671 and 1641 cm^{-1} (1670 and 1644 cm^{-1} in tuna cyt *c*) and extended-chain structures at 1641 and 1631 cm^{-1} (1644 and 1630 cm^{-1} in tuna cyt *c*) accompanies the loss of helical absorption in the three cyts *c*. New bands at ∼1616 and 1684 cm^{-1}, due

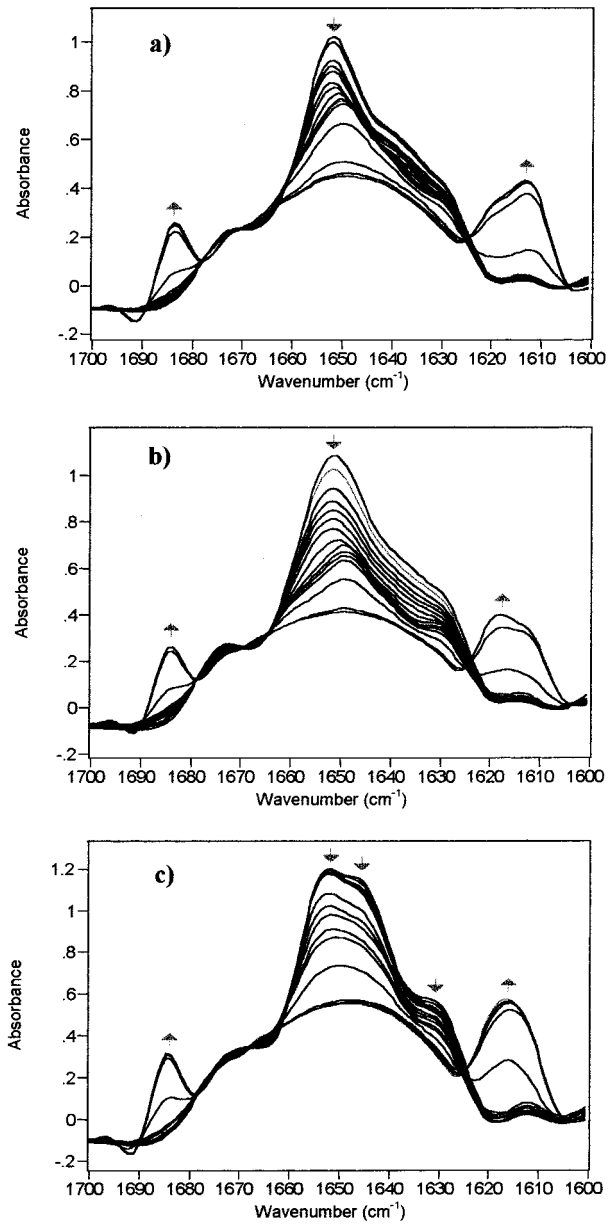

FIGURE 2: Stacked absorbance vs temperature (25−81 °C) plots of the deconvolved amide I′ (D_2O) bands of 4 mM (a) horse, (b) cow, and (c) tuna cyts *c* in 50 mM sodium phosphate buffer containing 0.2 M KCl (pD 7.0). Experimental details are given in the text. Vertical arrows represent an increase (↑) or decrease (↓) in the band intensity as the temperature is raised. The temperature interval per trace is 4 °C, and the data were plotted using Omnic 3.1 software (Nicolet). The aggregation bands (1616 and 1684 cm^{-1}) reach ∼1/3 their final intensities at 69, 73, and 65 °C in (a), (b), and (c), respectively.

to intermolecular antiparallel β-sheets resulting from irreversible aggregation of the unfolded protein (*19*, *21*, *22*), grow between 65 and 74 °C. The intensities of the bands at 1684 and 1616 cm^{-1} remained constant above 75 °C as seen in Figure 2. Upon cooling from 95 to 25 °C, the aggregation bands remained unchanged, demonstrating that the denaturation of the protein was irreversible (data not shown). The transition-midpoint temperatures (T_m) for aggregation and loss of secondary structure, as monitored by intensity changes in the amide I′ bands, overlap at 74 °C (bovine), 70 °C (horse), and 65 °C (tuna) in the 1D plots (*10*).

Only a limited amount of information on the sequence of unfolding events can be obtained from the 1D spectra. A more sensitive approach, such as resolution-enhanced 2D IR analysis, is required to detect minor out-of-phase variations due to noncooperative events during the thermal unfolding process (*16*). The assignments of the peaks in the 2D IR plots are summarized in Tables 1−3 and are discussed next.

Table 1: Correlation Table for the Deconvolved FTIR Spectra of Horse Cyt *c* over the Temperature Range 25−81 °C[a−e]

cm^{-1}	1684↑	1652↓	1647↓	1637↓
1630↓	−+⇒	++⇐	+ ⇔	++⇐
1637↓	−+⇒	+−⇒	+−⇒	
1647↓	−+⇒	++⇐		
1652↓	−+⇒			

Sequence of events for individual components

⇓
- turns / extended chains (1637 cm^{-1})↓
- less stable α-helices (1652 cm^{-1})↓
- extended chains (1630 cm^{-1})↓ and α-helices (1647 cm^{-1})↓
- intermolecular antiparallel β-sheet (1684 cm^{-1})↑

[a] Spectral data from Figure 2a. [b] Column and row headings represent the *X* and *Y* frequencies, respectively, from the 2D maps in Figure 3. [c] Vertical arrows represent an increase (↑) or decrease (↓) in the band intensity as the temperature is raised. [d] The signs (+, −) of the *X*, *Y* peaks above the diagonal in the 2D synchronous maps (left-hand sign) and asynchronous maps (right-hand sign) are indicated. [e] Horizontal arrows indicate the sequence of intensity changes: $Y \Rightarrow X$ and $Y \Leftarrow X$ denote that the intensity change at *Y* occurs at lower (⇒) or higher (⇐) temperature than that at *X*; $Y \Leftrightarrow X$ denotes that the intensity changes at *Y* and *X* are synchronous.

Table 2: Correlation Table for the Deconvolved FTIR Spectra of Cow Cyt *c* over the Temperature Range 25−81 °C[a−e]

cm^{-1}	1684↑	1652↓	1637↓
1630↓	−+⇒	++⇐	++⇐
1637↓	−+⇒	+−⇒	
1652↓	−+⇒		

Sequence of events for individual components

⇓
- turns / extended chains (1637 cm^{-1})↓
- α-helices (1652 cm^{-1})↓
- extended chains (1630 cm^{-1})↓
- intermolecular antiparallel β-sheet (1684 cm^{-1})↑

[a] Spectral data from Figure 2b. [b] Column and row headings represent the *X* and *Y* frequencies, respectively, from the 2D maps in Figure 4. [c−e] See footnotes to Table 1.

2D IR Correlation Plots of Horse Cyt c. In the synchronous 2D IR plot of horse cyt *c* (Figure 3a), three autocorrelation peaks (along the diagonal) centered at 1684, 1652, and 1616 cm^{-1} are observed, indicating that the relative intensities of these bands change with increasing temperature. The elongated autopeak centered at 1652 cm^{-1} in the synchronous plot (Figure 3a) is broad with low resolution, suggesting that additional peaks are buried underneath.

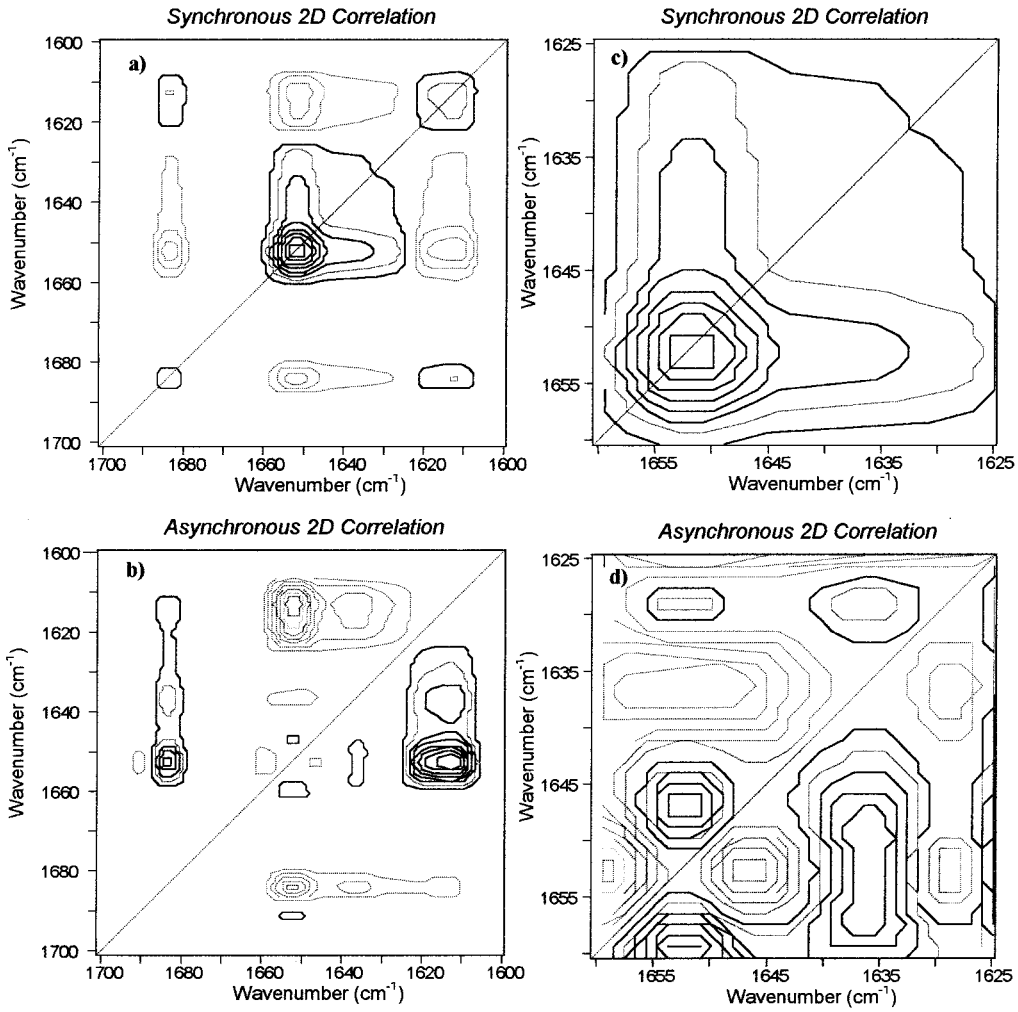

FIGURE 3: 2D IR (a, c) synchronous and (b, d) asynchronous maps of the amide I′ absorption of horse cyt *c* constructed from the spectral data in Figure 2a. 2D correlation plots were generated using KG2D software (*17, 18*) over the full amide I′ region (1600−1700 cm^{-1}) and the expanded helical region (1660−1625 cm^{-1}) to increase resolution. Solid and dashed lines represent positive and negative correlation peaks, respectively.

Table 3: Correlation Table for the Deconvolved FTIR Spectra of Tuna Cyt *c* over the Temperature Range 25−81 °C[a−e]

cm^{-1}	1684↑	1652↓	1646↓
1630↓	− + ⇐	+ − ⇐	+ − ⇐
1646↓	− + ⇐	+ − ⇐	
1652↓	− + ⇐		

Sequence of events for individual components

⇓

extended chains (1630 cm^{-1})↓

turns / extended chains (1646 cm^{-1})↓ and less stable α-helices c (1646 cm^{-1})↓

α-helices (1652 cm^{-1})↓

intermolecular antiparallel β-sheet (1684 cm^{-1})↑

[a] Spectral data from Figure 2c. [b] Column and row headings represent the *X* and *Y* frequencies, respectively, from the 2D maps in Figure 5. [c−e] See footnotes to Table 1.

Hence, a 3D representation of the 2D map was generated (data not shown), and, as expected, autopeaks at 1637 and 1630 cm^{-1} were detected. The positive cross-correlation peak at 1684 vs 1616 cm^{-1} indicates that the peak intensities assigned to aggregation are changing in the same direction. Likewise, positive intensity at 1652 vs 1637 cm^{-1} and at 1652 vs 1630 cm^{-1} indicates that the absorptions assigned to α-helices (1652 cm^{-1}), turns/extended-chains (1637 cm^{-1}), and extended-chains (1630 cm^{-1}) are changing in the same direction. Two negative cross-correlation peaks are observed at 1684 vs 1652 cm^{-1} and at 1652 vs 1616 cm^{-1}, revealing that the unfolding of α-helices (1652 cm^{-1}) is accompanied by protein aggregation (1684 and 1616 cm^{-1}).

Cross-correlation peaks in the asynchronous plot for horse cyt *c* (Figure 3b) indicate that peak intensities of some secondary structure components vary out-of-phase (i.e., are accelerated or delayed) with respect to each other as the temperature is increased. Thus, the thermal unfolding of horse cyt *c* involves sequential events that can be interpreted from the 2D IR correlation maps. Since the cross-correlation peaks at 1684 vs 1652 cm^{-1} and at 1684 vs 1637 cm^{-1} are positive in the asynchronous map but negative in the synchronous map, denaturation of α-helical (1652 cm^{-1}) and turns/extended-chains (1637 cm^{-1}) precedes protein aggregation (1684 cm^{-1}). The negative cross-correlation peaks in the asynchronous maps (1652, 1637, and 1630 vs 1616 cm^{-1})

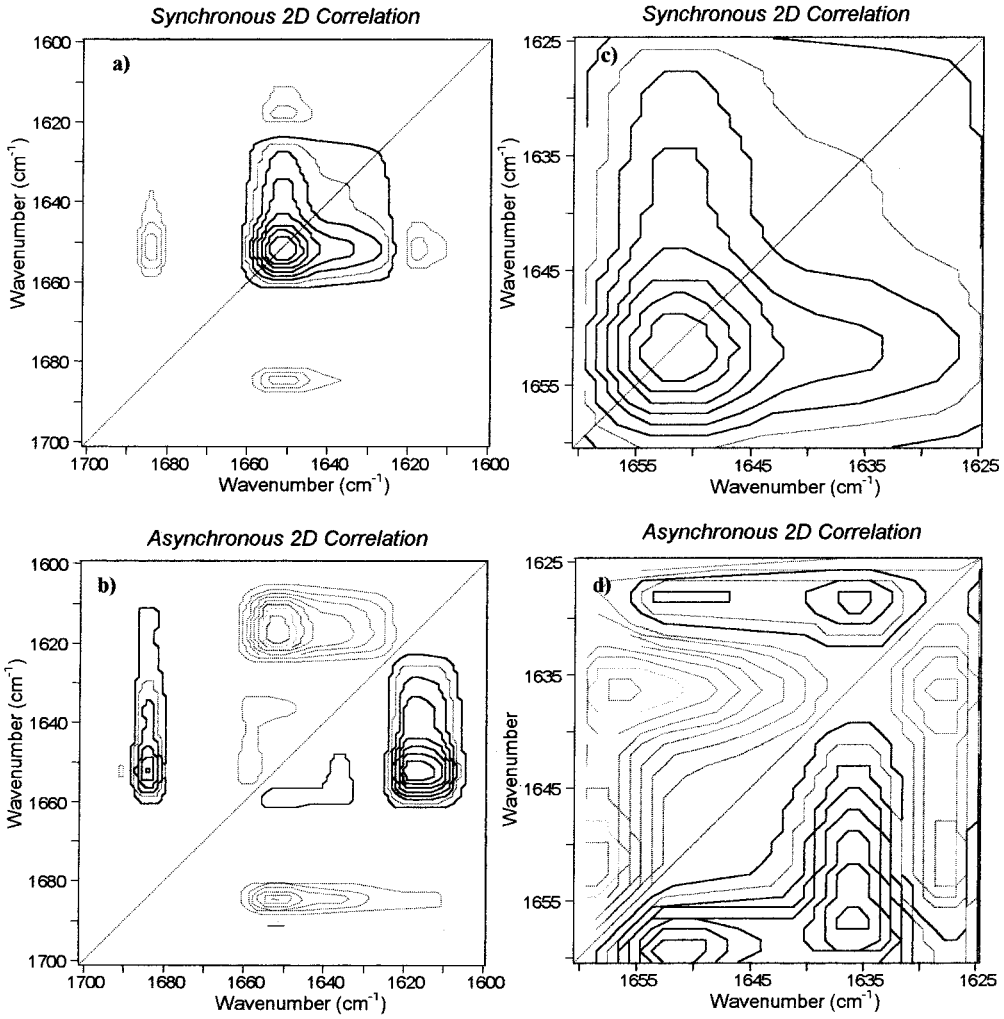

FIGURE 4: 2D IR (a, c) synchronous and (b, d) asynchronous maps of the amide I′ absorption of cow cyt *c* constructed from the spectral data in Figure 2b. See caption to Figure 3.

can be interpreted in a similar manner, with the secondary structure elements denaturing at lower temperature than protein aggregation. Thus, despite the apparent overlap of their T_m values in the 1D integrated intensity vs temperature plots (*10*), loss of secondary structure and protein aggregation are not synchronous events in horse cyt *c*.

To examine the sequential thermal unfolding of secondary structures in horse cyt *c* (Figure 1) in greater detail, a set of synchronous and asynchronous plots with higher resolution were generated over the range 1660−1625 cm^{-1} (Figure 3c,d). In the asynchronous map, the positive cross-peak (1652 vs 1630 cm^{-1}) reveals that the α-helices (1652 cm^{-1}) unfold before denaturation of the extended-chains (1630 cm^{-1}), whereas the negative cross-peak (1652 vs 1637 cm^{-1}) indicates that disruption of turns/extended-chains (1637 cm^{-1}) occurs before loss of α-helical structures (1652 cm^{-1}). Moreover, a positive peak at 1637 vs 1630 cm^{-1} reveals denaturation of turns/extended-chain structures (1637 cm^{-1}) prior to extended-chains (1630 cm^{-1}). A positive cross-correlation peak (1652 vs 1647 cm^{-1}) exposes the existence of a 1647-cm^{-1} band, which we assign to low-frequency α-helices, based on previous curve-fitting of the 1D spectra (*10*). Hence, unfolding of α-helical components in horse cyt *c* does not occur simultaneously but sequentially, with the helices that absorb at higher frequency denaturing at lower temperature.

The sequence of intensity changes of peaks assigned to the secondary structural elements (Figure 1) in the thermal denaturation of horse cyt *c* is summarized in Table 1. Recently, NMR H/D-exchange experiments performed on native horse cyt *c* implicated a sequential unfolding pathway, where unfolding of cooperative structural units occurs as a function of temperature (*23, 24*). It was proposed that global unfolding is initiated by unfolding of the cooperative unit containing residues 71−85, followed by a loop between residues 36−61; these changes are consistent with the initial loss in intensity we observe at 1637 cm^{-1} (turns/extended-chain). Next, the 60s helix (residues 61−70) and a region between residues 20−35 denature as a cooperative unit, which can be associated with the 1652- and 1630-cm^{-1} absorption bands, respectively. The final transition to the globally unfolded state is marked by the simultaneous unfolding of the N-terminal (residues 3−12) and C-terminal (residues 90−100) helices (*23, 24*), consistent with the unfolding of low-frequency α-helices (1647 cm^{-1}) transpiring before the onset of aggregation at 1684 and 1616 cm^{-1} (Table 1).

2D IR Correlation Plots of Cow Cyt c. Due to their high sequence identity and similar local and global stabilities (*7, 8, 10, 25*), one would expect the sequence of unfolding events to be very similar for horse and cow cyts *c*. The

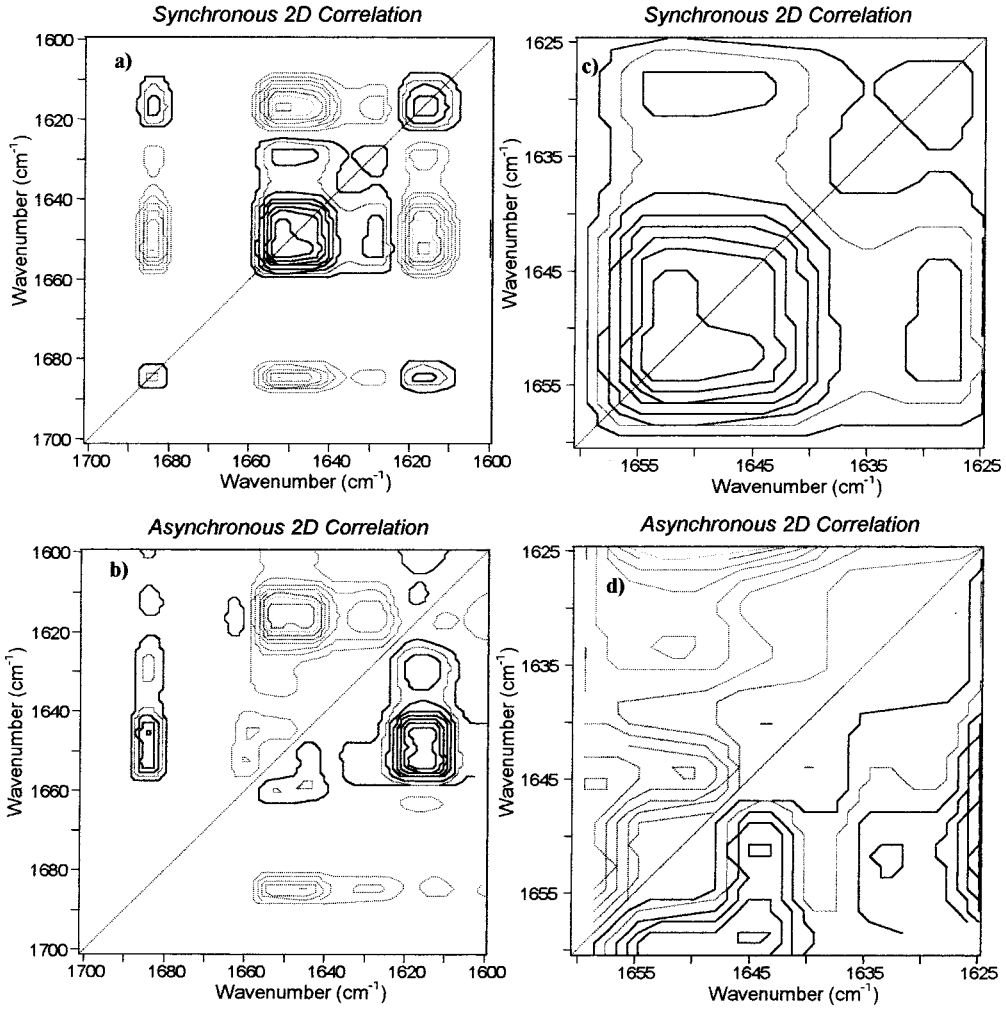

FIGURE 5: 2D IR (a, c) synchronous and (b, d) asynchronous maps of the amide I′ absorption of tuna cyt *c* constructed from the spectral data in Figure 2c. See caption to Figure 3.

synchronous map of cow cyt *c* (Figure 4a) reveals essentially the same broad autopeak centered at 1652 cm^{-1} detected for horse cyt *c* (Figure 3a). Autopeaks at 1637 and 1630 cm^{-1} are detected when a 3D representation of the 2D map is plotted (data not shown), and the improved resolution afforded by the 3D representation revealed additional autopeaks (1684 and 1616 cm^{-1}), as seen in the horse cyt *c* 2D map (Figure 3a). Negative cross-correlation peaks at 1684 vs 1652 cm^{-1} and at 1652 vs 1616 cm^{-1} indicate that α-helical intensity (1652 cm^{-1}) changes in the opposite direction to aggregation (1684 and 1616 cm^{-1}). Positive intensity at 1652 vs 1637 and 1630 cm^{-1} reveals that the absorption at 1652 cm^{-1} (α-helices) changes in the same direction as that centered at 1637 (turn/extended-chain) and 1630 cm^{-1} (extended-chain). In summary, from the 2D synchronous plot of cow cyt *c*, it can be concluded that as the temperature is increased, denaturation of turn/extended-chain (1637 cm^{-1}), α-helical (1652 cm^{-1}), and extended-chain (1630 cm^{-1}) structures is accompanied by protein aggregation (1684 and 1616 cm^{-1}) as was observed for horse cyt *c*.

An elongated positive cross-correlation peak (1684 vs 1652, 1637, and 1630 cm^{-1}) and a broader elongated negative cross-correlation peak (1652, 1637, and 1630 vs 1616 cm^{-1}) are detected in the asynchronous plot of cow cyt *c* (Figure 4b). Hence, aggregation (1684 and 1616 cm^{-1}) of cow cyt *c* also occurs at higher temperature following denaturation of its α-helices (1652 cm^{-1}), turn/extended-chain (1637 cm^{-1}), and extended-chain structures (1630 cm^{-1}). However, the absence of an α-helical cross-peak (1652 vs 1647 cm^{-1}) in the high-resolution asynchronous map of cow cyt *c* (Figure 4d) reveals cooperative unfolding of *all* its α-helical structures. This must be due to the three amino acid substitutions in cow cyt *c*, two of which actually occur in helical segments: Lys60 (horse) → Gly60 (cow) and Thr89 (horse) → Gly89 (cow). The third substitution is in a loop region, Thr47 (horse) → Ser47 (cow).

Table 2 summarizes the correlation peaks observed in the synchronous and asynchronous maps of cow cyt *c*, and the sequence of the thermally induced intensity changes that reveal the sequential events in unfolding. Initially there is disruption of extended-chain and/or turn structures (1637 cm^{-1}) followed by the cooperative unfolding of the helical components (1652 cm^{-1}), then denaturation of extended-chain structures (1630 cm^{-1}). The appearance of aggregation bands (1684 and 1616 cm^{-1}) at higher temperature establishes that the protein is denatured. Thus, using the 2D IR approach, global-stability variations between horse and cow cyts *c* (*7, 8, 10, 25*) can be pinpointed to differences in the unfolding sequence of their helical structures (Table 1 vs 2), which renders the cow protein more thermally stable than the horse protein.

2D IR Correlation Plots of Tuna Cyt c. The 1D stacked (Figure 2c) and 2D synchronous (Figure 5a) plots reveal that helices (1652 and 1646 cm^{-1}), turns (1646 cm^{-1}), extended-chain structures (1646 and 1630 cm^{-1}), and aggregation bands (1616 and 1684 cm^{-1}) change in intensity with increasing temperature as seen for horse and cow cyts *c*. The presence of cross-correlation peaks in the asynchronous plot (Figure 5b) indicates that the various structural components of tuna cyt *c* respond differently to increasing temperature as summarized in Table 3. Elongated positive asynchronous cross-peaks (1685 vs 1652, 1646, and 1630 cm^{-1}) and corresponding negative synchronous peaks (Figure 5a) imply that helical (1652 and 1646 cm^{-1}), turn (1646 cm^{-1}), and extended-chain (1646 and 1630 cm^{-1}) structures denature prior to aggregation (1684 cm^{-1}) as in horse and cow cyts *c*.

Several weak cross-correlation peaks are observed in the high-resolution 2D correlation maps (1625−1660 cm^{-1}) of tuna cyt *c* (Figure 5c,d). For instance, negative correlation peaks at 1652 vs 1630 cm^{-1} and at 1646 vs 1630 cm^{-1} in the asynchronous plot (Figure 5d) reveal that low-frequency extended-chain structures (1630 cm^{-1}) lose intensity before the α-helices, contrary to what was found for horse and cow cyts *c*. Furthermore, the negative correlation peak at 1652 vs 1646 cm^{-1} indicates that the low-frequency helices (1646 cm^{-1}) unfold before the high-frequency helices (1652 cm^{-1}), which is opposite to that observed for horse cyt *c* (Table 1 vs 3). Curve-fitting of the 1D spectra (*10*) revealed splitting of the helical absorption in tuna cyt *c* with ∼20% intensity at the lower frequency. In contrast, splitting of the helical absorption of horse cyt *c* was only detected using the more sensitive 2D analysis (Figure 3d), but even this approach failed to detect helical splitting in cow cyt *c* (Figure 4d). Since H-bonding of the peptide carbonyl red-shifts the amide I′ absorption (*26*), low-frequency helices are more strongly H-bonded and/or more solvent-exposed than those at higher frequencies. Red-shifting of the helical absorption in tuna *c* has been attributed to increased solvent exposure, yielding helices that are less stable and unfold at lower temperature than the more buried helices with 1652-cm^{-1} absorption (*10*). Following loss of secondary structure, protein aggregation occurs, giving rise to bands at 1684 and 1616 cm^{-1}.

The difference in the sequence of unfolding events in tuna compared to horse and cow cyts *c* can ultimately be linked to the less stable heme-crevice of the tuna protein (*7*, *10*). Using mass spectrometry to monitor H/D exchange in horse cyt *c*, Zhang and Smith (*27*) observed that residues 29−33 (Figure 1), which form an extended-chain structure adjacent to the heme, are shielded from the solvent. Assuming that residues 29−33 contribute to the low-frequency extended-chain absorption (1630 cm^{-1}) of tuna cyt *c*, their denaturation before α-helices (Table 3) would be consistent with the significantly decreased stability of the heme crevice in tuna vs horse or cow cyts *c* (*7*, *10*).

In summary, subtle but significant differences in the sequence of thermal unfolding events are detected by 2D correlation analysis of the FTIR spectra of horse, cow, and tuna cyts *c* shown in Figure 2. Despite their high sequence identity (>97%), horse and cow cyts *c* exhibit nonidentical thermal unfolding pathways, with helical structures denaturing sequentially in horse cyt *c*, but cooperatively in cow cyt *c* (Table 1 vs 2). The first step in tuna cyt *c* thermal denaturation involves alteration of low-frequency extended-chain structures (Table 3), which include residues 29−33 in the heme-crevice region (Figure 1); in contrast, this is the most stable region in horse cyt *c* (*27*) and very likely in cow cyt *c* also (Table 2). Hence, decreased stability of the heme crevice in tuna cyt *c* (*7*, *8*, *10*) determines the sequence of unfolding events as the temperature is increased. Nevertheless, variations in local stability and unfolding do not have a dramatic affect on overall stability, since the global unfolding of all three cyts occurs within a narrow 10 °C range (65−75 °C) (*8*, *10*). It is also of note that the overlapping T_m values for the global stability obtained from the 1D FTIR analyses (*10*) suggested that loss of secondary structure and aggregation occur in parallel, but the 2D analyses clearly show that these are sequential events; the denatured proteins aggregate, rather than aggregation promoting denaturation.

CONCLUSIONS

Using a highly homologous set of proteins, horse, cow, and tuna cyts *c*, with solved X-ray (*2*, *5*) and NMR (*4*, *6*) structures, we have demonstrated the power of resolution-enhanced 2D IR correlation analysis in identifying the relative stabilities of secondary structures. The results are consistent with those from NMR H/D-exchange experiments performed on horse cyt *c*, which reveal that specific structural units unfold cooperatively (*23*, *24*). The present study also illustrates the usefulness of resolution-enhanced 2D IR correlation analysis in detecting subtle changes in structural components and in uncovering sequential events in unfolding following thermal perturbation. Clearly, a powerful feature of this approach is the ability to distinguish between structural elements with overlapping absorption (*16*, *17*) such as α-helices of varying stabilities. In future studies, one can envision modifying key structural residues to relate differences found by 2D IR correlation analysis in unfolding/refolding pathways to specific sites. Furthermore, since the acquisition of FTIR spectra is rapid and requires little sample and FTIR equipment is relatively inexpensive, 2D IR screening should provide an invaluable tool for identifying candidate proteins for structure determination by NMR or X-ray crystallography in whole-proteome studies.

REFERENCES

1. Dickerson, R. E. (1980) *Sci. Am. 242*, 137−153.
2. Bushnell, G. W., Louie, G. V., and Brayer, G. D. (1990) *J. Mol. Biol. 214*, 585−595.
3. Moore, G. R., and Pettigrew, G. W. (1990) *Cytochromes c—Evolutionary, Structural and Physiochemical Aspects*, Springer-Verlag, Berlin.
4. Moore, G. R., and Williams, R. J. (1980) *Eur. J. Biochem. 103*, 533−541.
5. Takano, T., and Dickerson, R. E. (1981) *J. Mol. Biol. 153*, 79−94.
6. Gao, Y., Lee, A. D., Williams, R. J., and Williams, G. (1989) *Eur. J. Biochem. 182*, 57−65.
7. Filosa, A., and English, A. M. (2000) *J. Biol. Inorg. Chem. 5*, 448−554.
8. Endo, S., Nagayama, K., and Wada, A. (1985) *J. Biomol. Struct. Dyn. 3*, 409−421.
9. Hu, Y., Fenwick, C., and English, A. M. (1996) *Inorg. Chim. Acta 242−243*, 1−9.
10. Filosa, A., Ismail, A. A., and English, A. M. (1999) *J. Biol. Inorg. Chem. 4*, 717−726.

11. Schejter, A., Luntz, T. L., Koshy, T. I., and Margoliash, E. (1992) *Biochemistry 31*, 8336−8343.
12. Kaminsky, L. S., Miller, V. J., and Davison, A. J. (1973) *Biochemistry 12*, 2215−2221.
13. Pettigrew, G. W., Aviram, I., and Schejter, A. (1975) *Biochem. J. 149*, 155−167.
14. Yuan, X., Hawkridge, F. M., and Cheblowski, J. F. (1993) *J. Electroanal. Chem. 350*, 29−42.
15. Noda, I. (1993) *Appl. Spectrosc. 47*, 1329−1336.
16. Fabian, H., Mantsch, H. H., and Schultz, C. (1999) *Proc. Natl. Acad. Sci. U.S.A. 96*, 13153−13158.
17. Ismoyo, F., Wang, Y., and Ismail, A. A. (2000) *Appl. Spectrosc. 54*, 939−947.
18. Wang, Y., Murayama, K., Myojo, Y., Tsenkova, R., Hayashi, N., and Ozaki, Y. (1998) *J. Phys. Chem. B 102*, 6655−6662.
19. Ismail, A. A., Mantsch, H. H., and Wong, P. T. T. (1992) *Biochim. Biophys. Acta 1121*, 183−188.
20. Jackson, and Mantsch, H. H (1995) *Crit. Rev. Biochem. Mol. Biol. 30*, 95−120.
21. Clark, A. H., Saunderson, D. H., and Suggett, A. (1981) *Int. J. Pept. Protein Res. 17*, 353−364.
22. Boye, J. I., Alli, I., Ismail, A. A., Gibbs, B. F., and Konishi, Y. (1995) *Int. Dairy J. 5*, 337−353.
23. Bai, Y., Sosnick, T. R., Mayne, L., and Englander, S. W. (1995) *Science 269*, 192−197.
24. Milne, J. S., Xu, Y., Mayne, L. C., and Englander, S. W. (1999) *J. Mol. Biol. 290*, 811−822.
25. McLendon, G., and Smith, M. (1978) *J. Biol. Chem. 253*, 4004−4008.
26. Haris, P. I., and Chapman, D. (1992) *Trends Biochem. Sci. 17*, 328−333.
27. Zhang, Z., and Smith, D. L. (1993) *Protein Sci. 2*, 522−531.

BI002710N